Contents lists available at ScienceDirect

Corrosion Science

The self-sustaining propagation of crevice corrosion on the hybrid BC1 Ni–Cr–Mo alloy in hot saline solutions

N. Ebrahimi [a], J.J. Noël [a], M.A. Rodríguez [b], D.W. Shoesmith [a],*

[a] Department of Chemistry and Surface Science Western, The University of Western Ontario, London, Ontario, Canada
[b] Gerencia Materiales, CNEA, CONICET, Instituto Sabato, UNSAM/CNEA, Buenos Aires, Argentina

ARTICLE INFO

ABSTRACT

The initiation and propagation of crevice corrosion on the BC1 nickel-chromium-molybdenum alloy has been studied galvanostatically in concentrated chloride solution at 120 °C, and the distribution of corrosion damage determined using surface analytical techniques. The distribution of damage was dependent on the applied current and showed an increased tendency to spread across the surface as the applied current was increased. Attempts to induce repassivation by galvanodynamically reducing the current to zero were unsuccessful. Galvanic coupling to a large BC1 counter electrode showed propagation could be maintained by oxygen reduction on the coupled electrode at a slow rate for >1200 h.

© 2016 Elsevier Ltd. All rights reserved.

1. Introduction

The ability of nickel to retain large amounts of different alloying elements in solid solution has stimulated the development of several binary, ternary and other complex Ni-based families of alloys [1,2], with each family designed for specific applications. Commercially pure Ni is widely used in caustic environments, and addition of Cu to Ni improves its corrosion resistance in reducing environments, such as hydrofluoric acid, but the corrosion resistance in oxidizing media is poor [2,3]. Ni–Mo alloys show excellent resistance to reducing acids (HCl and H_2SO_4) even at elevated temperature but the lack of Cr makes them susceptible to corrosion in the presence of oxidizing species such as ferric and cupric ions and dissolved oxygen. Ni–Cr–Mo alloys were designed to extend corrosion resistance to both reducing and oxidizing environments, with the Hybrid-BC1 developed to fill the gap between Ni–Mo and Ni–Cr–Mo alloys [4–6]. This alloy has a better resistance to reducing environments than the Ni–Cr–Mo alloys, but also resists corrosion under oxidizing conditions and has a high resistance to localized corrosion. These properties make the BC1 alloy suitable for a wide range of applications in the chemical processing, pharmaceutical, agricultural, food, petrochemical and power industries [7,8].

The reliable performance of Ni–Cr–Mo alloys under extreme industrial conditions is generally attributed to the presence of a passive film on the alloy surface [9–12]. However, under localized corrosion conditions when this film is breached, the alloying elements play a major role in controlling propagation and inducing repassivation. While the crevice corrosion of a range of Ni–Cr–Mo alloys has been studied [13–17], information on the crevice corrosion of the BC1 alloy is sparse. A recent comparison [4] of the C22 (Ni-22Cr-13Mo-3W) and BC1 (Ni-15Cr-22Mo) alloys in a 1 M HCl solution (90 °C), simulating the conditions inside an active crevice, showed that, while the current density for active dissolution was lower, the passive current density on the high-Mo BC1 was greater than that on the high-Cr C22. Crevice repassivation potentials ($E_{R,Crev}$) for the two alloys showed that the BC1 alloy repassivated at higher potentials, indicating a beneficial effect of Mo on repassivation.

Recent studies on a wide range of Ni–Cr–Mo alloys showed that their resistance to crevice corrosion, based on breakdown and repassivation potentials and protection temperatures, improved as the Mo content increased [15,18,19]. In many of these studies the potentiodynamic–galvanostatic–potentiodynamic (PD–GS–PD) technique [20] was used to measure breakdown and repassivation potentials. While this technique provides fast and reliable measurements of the susceptibility to crevice corrosion, allowing the

* Corresponding author at: University of Western Ontario, Depertment of Chemistry, 1151 Richmond Street, London, Ontario N6A 5B7, Canada Fax: +1 519 661 3022.
E-mail address: dwshoesm@uwo.ca (D.W. Shoesmith).

Table 1
Chemical composition (wt.%) of BC1 alloy provided by Haynes International Co.

Alloy/Element	Ni	Cr	Mo	Fe	C	Mn	Si
BC1	62	15	22	2	0.01	0.25	0.08

expected corrosion performance of various alloys to be ranked, it does not provide significant mechanistic information.

In this study, a combination of galvanostatic and galvanic-coupling techniques has been applied to study the various stages of crevice corrosion (initiation/activation, propagation and repassivation), with the primary goal of investigating the influence of the decreased Cr and increased Mo content of the BC1 alloy (Ni-15Cr-22Mo) compared to the well-studied C22 alloy (Ni-22Cr-13Mo-3W).

The galvanostatic technique has been used [16,21,22] to study a number of Ni–Cr–Mo alloys. The use of galvanostatic control guarantees initiation and prevents repassivation. This allows the propagation process to be investigated under conditions where both the rate of the external cathodic reaction and the total extent of electrochemically-inflicted damage can be controlled. Using the galvanic coupling technique previously used to study titanium alloys [23,24], in which a creviced electrode is galvanically coupled to a large counter electrode of the same material, all stages of the crevice corrosion process can be monitored. However, our previous studies [21,25] have shown that it is difficult to initiate crevice corrosion on Ni–Cr–Mo alloys under these natural corrosion conditions. In this study the galvanic coupling technique is used to follow the later stages of propagation (initiated galvanostatically) and repassivation.

2. Materials and methods

2.1. Experimental arrangement

The composition of the Hybrid-BC1 Ni–Cr–Mo alloy is given in Table 1. Specimens were cut from mill annealed sheets supplied by Haynes International (Kokomo, IN, USA). The specimens had a thickness of 3.17 mm and were bent in to a V shape to produce an artificial creviced assembly. A small polytetrafluoroethylene (PTFE) wafer was used to produce a single crevice with an area of $\sim$4 cm^2. The crevice tightness was adjusted using a PTFE "feeler" strip. The crevice electrode design and assembly have been described elsewhere [16,21]. Prior to each experiment, the crevice face and crevice former were ground with wet SiC papers from a 320 to a 1200 grit finish. All parts of the crevice assembly were rinsed in de-ionized (DI) water and sonicated in ethanol for 10 min.

All measurements were performed in 5 M NaCl solutions prepared using reagent grade NaCl crystals (Caledon Chemicals) and Type 1 water with a resistivity of 18 MΩ.cm. Prior to each experiment, the solution was vigorously agitated to ensure saturation with air. All experiments were performed at 120 °C inside a cylindrical pressure vessel modified as an electrochemical cell. A Teflon liner was used to prevent contact of the electrolyte with the pressure vessel body. All measurements were made using a homemade Ag/AgCl electrode in saturated KCl solution (-45 mV vs. SCE) with

the reference electrolyte solution contained within a PTFE container [26]. The counter electrode was of the same material as the working electrode, with a surface area $\sim$50 times bigger than that of the creviced electrode to simulate the small anode/large cathode geometry generally prevailing during localized corrosion [27,28]. In galvanic coupling experiments, a BC1 planar electrode, 20 mm in length and 5 mm in width and thickness, was used to reveal the difference in corrosion potential (E_{CORR}) between the creviced/counter electrode couple and a sample of the same material with no crevice. Before heating, the pressure vessel was tested for leaks by pressurizing with UHP (Ultra High Pressure) N$_2$ gas. After the cell was heated to the desired temperature and the crevice electrode potential (E_C) had stabilized, electrochemical measurements were performed.

2.2. Electrochemical measurements

Both galvanostatic and galvanodynamic polarization techniques were used to probe the crevice corrosion behavior of the BC1 alloy. In galvanostatic experiments, a charge of 6.9 C was applied to the working electrode by passing anodic currents of 80 μA, 40 μA, 20 μA or 10 μA for 24 h, 48 h, 96 h or 192 h, respectively. The potential response was measured using a WaveDriver 20 bipotentiostat (Pine Instrument Company).

In galvanodynamic polarization experiments, E_C was measured as the current was decreased from a set value (80 μA) at a constant rate of -0.464 nA/s. In other experiments, both galvanodynamic polarization and galvanic coupling were employed; after the current was ramped to zero, the creviced electrode was coupled to the counter electrode through a zero-resistance ammeter (Keithley model 6514), and the current flowing between the electrodes (I_C) recorded. During this coupling, E_C and the potential of the planar electrode (E_P) were measured with a high input impedance analogue-to-digital converter (ADC) (Iotech, ADC 488/16A). After 36 days, O$_2$ was added to the cell and E_C/I_C measurements continued.

Potentiodynamic polarization experiments were performed in a deaerated simulated crevice solution (1 M HCl + 4 M NaCl, pH 0) at 120 °C. E_{CORR} was measured for 20 min to ensure a stable surface condition and then a potential scan was applied at a rate of 0.167 mV/s. Scans were started from $E_{CORR}-50$ mV and extended up to a value at which an abrupt increase in anodic current density occurred.

2.3. Post-corrosion surface analysis

When each experiment was completed, the creviced specimen was rinsed in deionized water and ethanol, and dried using UHP Ar gas. The specimen was then photographed using a digital camera and image analysis software (Image Pro Plus) was used to analyze the creviced surface. A Hitachi S-4500 field emission scanning electron microscope (SEM) equipped with an EDAX^{TM} energy-dispersive X-ray spectroscopy (EDS) system was used to examine the surface features and to analyze the composition of the corroded sample.

Surface profilometry was used to obtain a 3 dimensional (3D) image of the corroded area and to measure the penetration depth in the corroded region. A mechanical stylus profilometer with a diamond tip ($\sim$2 μm in radius) was scanned over the surface at a speed of 50 μm/s. By stitching together the profiles obtained from a series of line scans over the surface, a 3D topographic image of the corroded area was reconstructed [15].
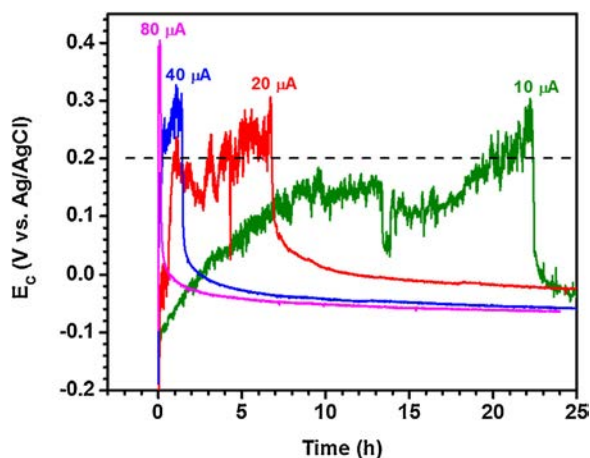
Table 2
Area corroded after the galvanostatic application of a charge of 6.9 C to the creviced sample in 5 M NaCl solution at 120 °C.

Applied current (μA)	Time (h)	Charge (C)	Corroded surface area (mm^2)
10	192	6.9	10.43
20	96	6.9	19.66
40	48	6.9	34.18
80	24	6.9	62.55

Fig. 1. First 25 h of the E_C vs. time plots recorded on the BC1 alloy at various applied currents in 5 M NaCl solution at 120 °C. The dashed line shows the 0.2 V thresholds for the onset of the passive-to-active transition [23].

Fig. 2. The steady-state crevice potential, (E_C) ss, (from Fig. 1) as a function of applied current.

3. Results and discussion

3.1. Crevice corrosion under galvanostatic polarization

Fig. 1 shows E_C for the first 25 h of experiments at 4 different values of applied current. As discussed previously [22], these curves Exhibit 3 distinct regions; (i) an initial rise in E_C as the passive film, comprising an inner Cr(III)/Ni(II) barrier layer and an outer Mo(VI) layer [29–32], is forced to grow by the applied current; (ii) a rapid decrease in E_C as the passive-to-active transition occurs; and (iii) the establishment of a steady-state E_C once active propagation conditions are established within the crevice. While these curves are similar in overall form to those previously recorded on C22 [21], they differ quantitatively. Though noisy, E_C does not exhibit the major potential excursions observed on C22. This can be attributed to the high Mo content in BC1 which suppresses the attempted activation events, observed as large transitory decreases in E_C on C22, by the rapid formation of molybdates at the film breakdown sites. The ability of Mo to repair attempted breakdown sites rapidly would also explain the longer times required to initiate the passive-to-active transition on BC1 (e.g., ∼22 h at an applied current of 10 μA, compared to ∼7 h for C22 at the same current) [16,21]. These observations are consistent with the metastable behavior on Ni–Cr–Mo alloys observed by others [32,33].

Except for the largest applied current (80 μA), the passive-to-active transition occurs once E_C reaches a value in the range 200 mV to 300 mV vs. Ag/AgCl. This is consistent with previous results for C22 which showed the initiation of crevice corrosion requires the onset of the transpassive conversion of the passive Cr(III) layer to Cr(VI), leading to the destruction of the passive film barrier layer. A combination of electrochemical impedance spectroscopy [21,34], X-ray photoelectron spectroscopy, and time-of-flight secondary ion mass spectrometry [30] showed this occurs for potentials ≥200 mV, as indicated by the dashed line in Fig. 1.

Once the passive-to-active transition has occurred the noise associated with E_C effectively disappears, indicating that once active conditions have been established, the applied current is used in propagation, not the initiation of additional active sites. This is consistent with previous observations on a number of alloys, which exhibit only one propagating site [22], and with the results of this study.

Although not shown in Fig. 1, E_C eventually reaches a steady-state value, $(E_C)_{SS}$, when stable propagation conditions are achieved within the creviced region, indicating the establishment of the critical crevice solution [35,36] and potential. $(E_C)_{SS}$ is the potential at
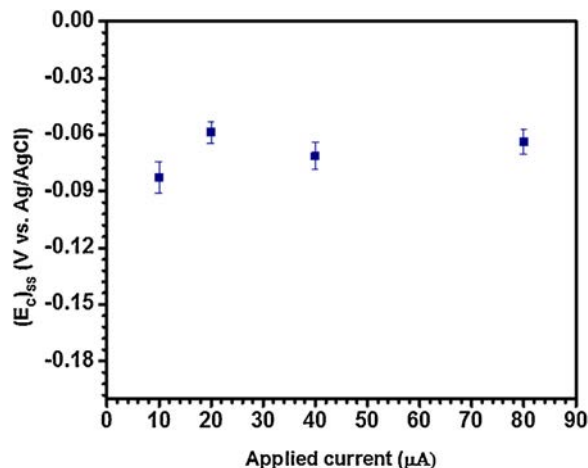
the mouth of the crevice, the actual potential at active locations within the crevice being lower as a consequence of the IR drop associated with the crevice [37]. Fig. 2 shows $(E_C)_{SS}$ is independent of the applied current over the range used in this study.

This independence indicates that the propagation process is not electrochemically controlled by the external current probably as a consequence of proton reduction inside the crevice as discussed previously [22]. In our previous study on the effects of alloying elements on crevice corrosion [22], $(E_C)_{SS}$ was shown to depend on the Mo content of a number of Ni–Cr–Mo alloys (including BC1), a feature which was shown to control the depth of corrosion penetration while making it effectively independent of the applied current for alloys with a sufficiently high Mo content.

3.2. Surface analyses of the corroded region

Fig. 3 shows optical images of the alloy corroded at different applied currents. The area covered with corrosion products is marked in red, and the dashed white lines indicate the edges of the crevice former. At some locations, particularly at an applied current of 10 μA, the red area extends to locations outside the creviced region. However, this is due to the transport and deposition of molybdate corrosion products from within the crevice and not due to corrosion at these external locations. At all currents, corrosion started close to the crevice edge and propagated both along the edge and toward the centre of the creviced area. As the current was increased, propagation along the edge dominated, as shown by the increase in the corroded region expanded along the crevice edge, while propagation into the crevice became independent of the applied current, Fig. 4, the latter indicating the external current is ineffective at these locations.

The total extent of crevice corrosion damage resulting from a constant applied charge in the form of different anodic currents is defined by the area of the surface corroded and the depth of penetration within that area. Table 2 shows the corroded areas, determined using Image Pro® software on optical images, as a function of applied current, the tendency for corrosion to spread as the applied current was increased being clearly apparent.

Fig. 5 shows a 3D image of the alloy surface after corrosion at an applied current of 20 μA (Fig. 3(b)). According to the IR drop model [38], to obtain an IR drop sufficiently large to place the surface in the active region, a short distance into the crevice from the crevice mouth should remain uncorroded. Beyond this depth the maximum penetration should be achieved at the location where the anodic dissolution current achieves a maximum. The location of maxi-
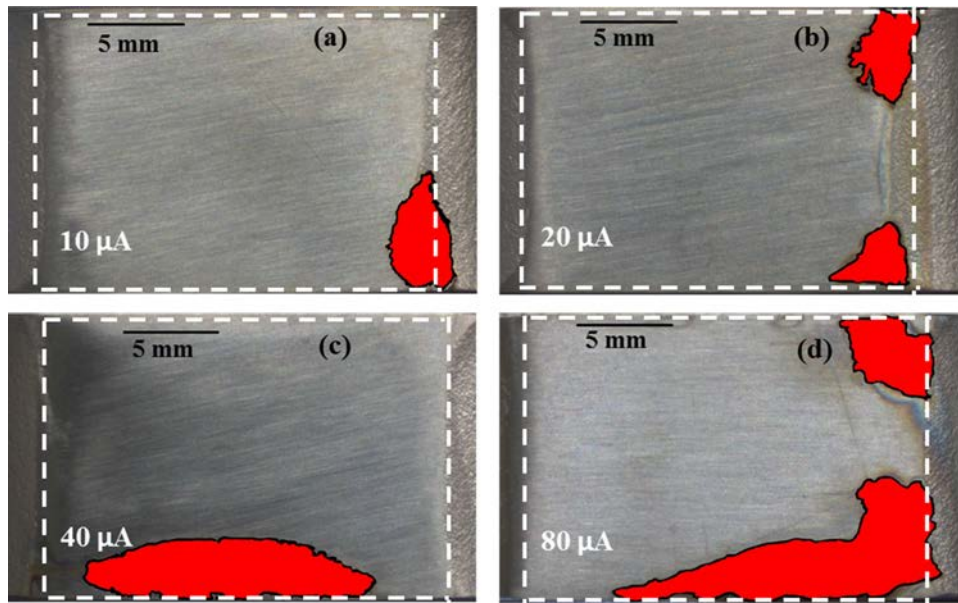
Fig. 3. Optical images of the surfaces after corrosion at different applied currents to a constant charge of 6.9 C; (a) 10 μA (192 h), (b) 20 μA (96 h), (c) 40 μA (48 h), and (d) 80 μA (24 h): the corroded region is coloured red, and the white dashed lines show the edge of the crevice. (For interpretation of the references to colour in this figure legend, the reader is referred to the web version of this article.)

mum penetration can be seen as the blue valley in the image, Fig. 5. However, the inner perimeter of the crevice does not exhibit a regular front easily interpretable according to the IR drop model. The images obtained for other applied currents show similar features, although the geometry tends to become more regular at the higher applied currents. As will be discussed in more detail below, these features reflect the redistribution of current as crevice propagation proceeds and corrosion product accumulates.

To obtain a measure of the depth of penetration, profilometry line scans were performed on samples that were corroded at the different applied currents, Fig. 6. In some cases, as shown in Fig. 3, the corrosion product was deposited outside the creviced region, and this deposit could not always be removed after the experiment, making it difficult to locate the uncorroded alloy surface by profilometry. This is particularly obvious in the line scans recorded at applied currents of 40 and 80 μA, Fig. 6((c) and (d)). This "offset" was taken into account when calculating penetration depths.

The depth profiles recorded as line scans are similar for samples corroded at all applied currents, Fig. 6. In all depth profiles,

the depth of damage increases with increasing distance from the crevice mouth, up to a maximum depth at a distance x_{Max}. Farther from the crevice mouth the depth decreases. However, a single line scan may not locate the actual point of maximum depth in the entire crevice, making the values only estimates. While x_{Max} is only qualitative, it is worth noting that it occurs closer to the crevice mouth as the applied current is increased, consistent with the expectations of the IR drop model [39–41].

Fig. 7 shows plots of the creviced areas and the maximum penetration depths obtained from images and profiles such as those in Fig. 3 and Fig. 6. As observed previously for alloy C22 [25], the area corroded increases and the penetration depth decreases as the applied current increases. However, for BC1 the area corroded is considerably larger ($10 mm^2$–$65 mm^2$) than for C22 ($1 mm^2$–$35 mm^2$) over the same current range for the same total charge (6.9 C). Correspondingly, the penetration depths are considerably smaller for BC1 (65–5 μm) than for C22 (82–20 μm). These results support our previous claim [22,25] that the redistribution of corrosion current over a wider area is driven by the accumulation
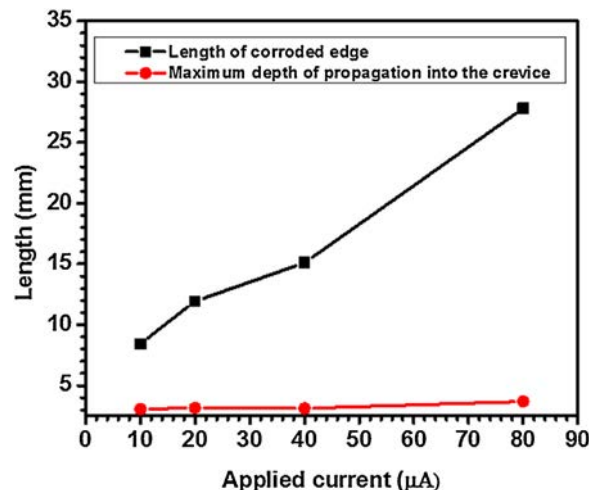

Fig. 4. The length of the corroded edge and the maximum depth of propagation into the crevice as function of the applied current.
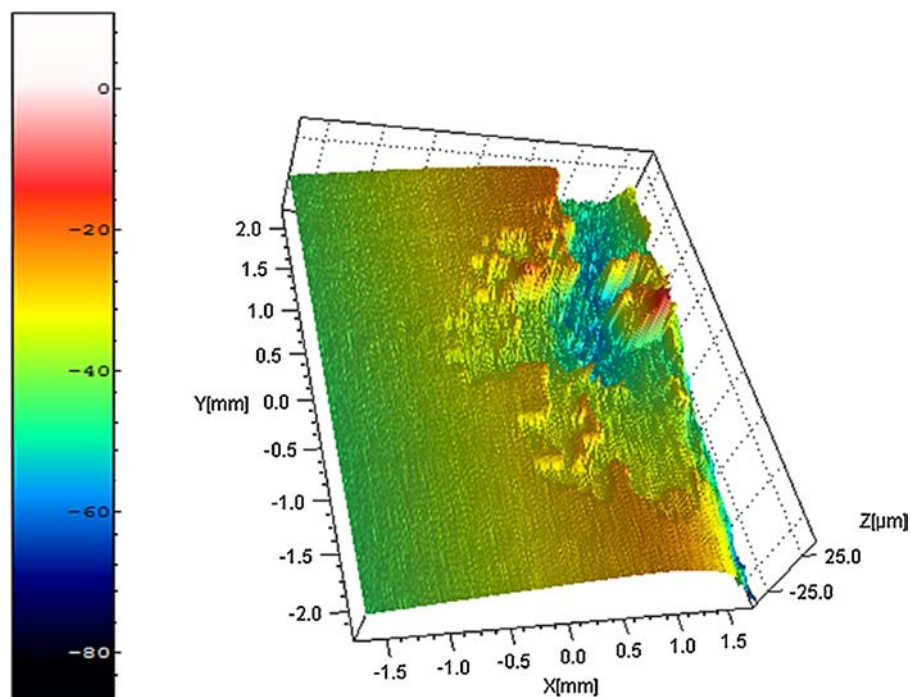
Fig. 5. 3D image obtained by profilometry on the BC1 crevice sample corroded at 20 μA for 96 h in 5 M NaCl solution at 120 °C. The scale shows the relationship between colour and depth.

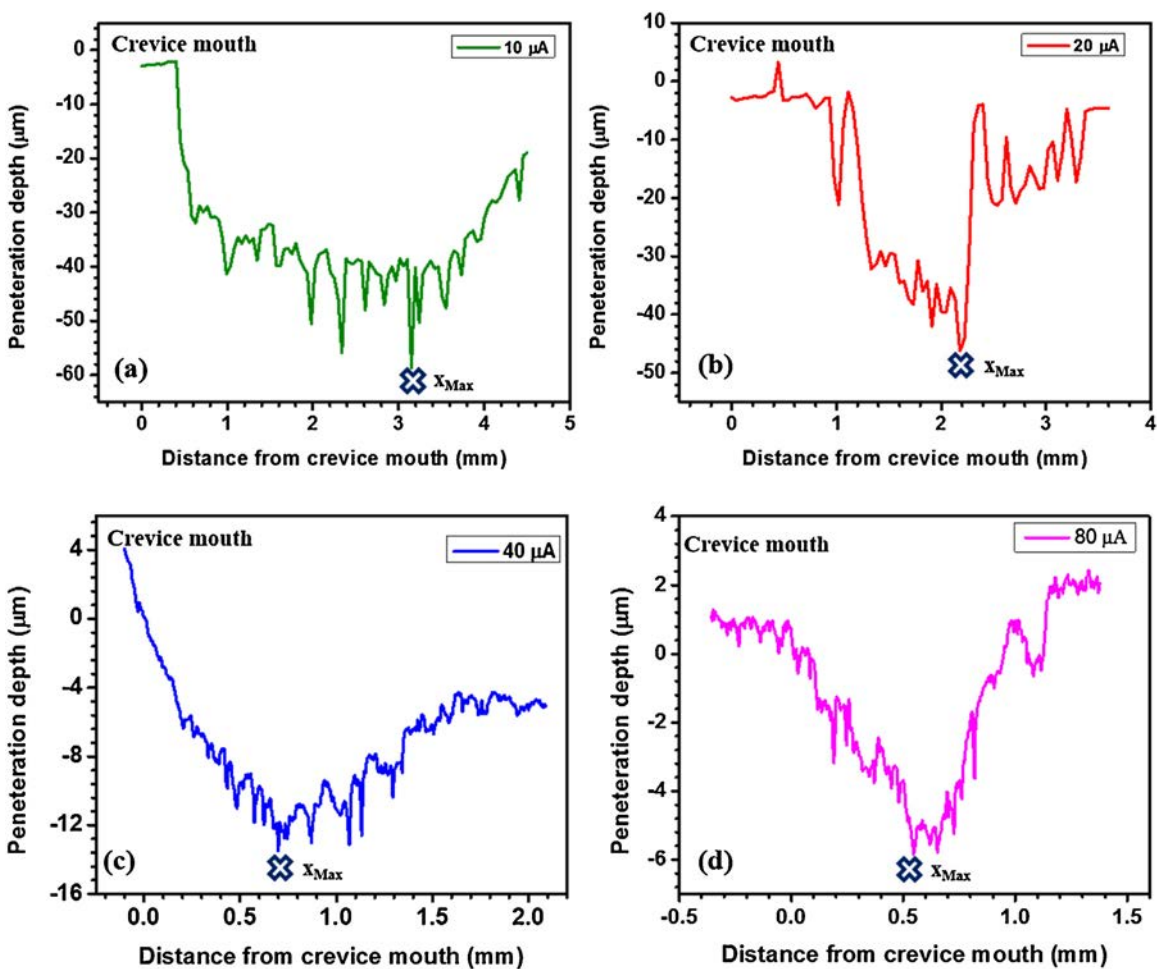**Fig. 6.** Line scans obtained by profilometry, showing the maximum penetration depth achieved under (x_{Max}) at (a) 10 μA, (b) 20 μA, (c) 40 μA, and (d) 80 μA. All depth measurements were made with respect to the crevice mouth, at which the depth was set to zero.
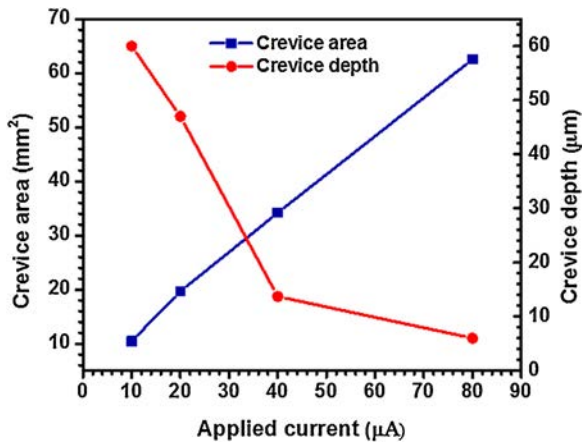
Fig. 7. Crevice area and maximum penetration depth as a function of applied current.

Fig. 9. The charge injection profiles for crevices corroded either galvanostatically or galvanodynamically.

of Mo oxides at the corroding location. These oxides insulate that location and force the current to relocate to areas unprotected by the presence of a molybdate deposit. As expected, this indication is more readily achieved for BC1 than for C22, due to the higher Mo content.

The presence of a Mo deposit is confirmed by the SEM image and EDS spectrum in Fig. 8. The flaky nature of the deposit and its high Mo content are consistent with previous observations [22,42] on crevice-corroded Ni–Cr–Mo alloys. At locations closer to the centre of the crevice where the deposit either detached or was removed, the pitted nature of the alloy surface can be seen (location 2, Fig. 8(c)). These pits are detected in the line scans shown in Fig. 6. Selective grain boundary attack has been shown to occur more readily on the random grain boundaries on Ni–Cr–Mo alloys,
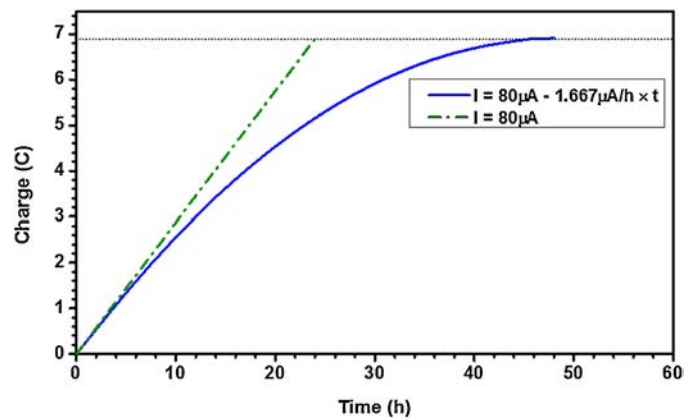
which have a large fraction of more corrosion resistant $\sum 3$ boundaries [43]. The deep penetration at triple points has been shown to be due to the higher susceptibility to corrosion of triple points between random boundaries [44,45].

3.3. Crevice repassivation

In galvanodynamic experiments, crevice corrosion was initiated at an initial applied current of 80 μA, and then the applied current was continuously decreased at a rate of 1.67 μA/h until the current reached 0. In this manner the same amount of charge (6.9 C) was injected as in the experiment at a continuously applied current of 80 μA. The rates of charge injection are compared in Fig. 9. By steadily decreasing the applied current in this manner, we might
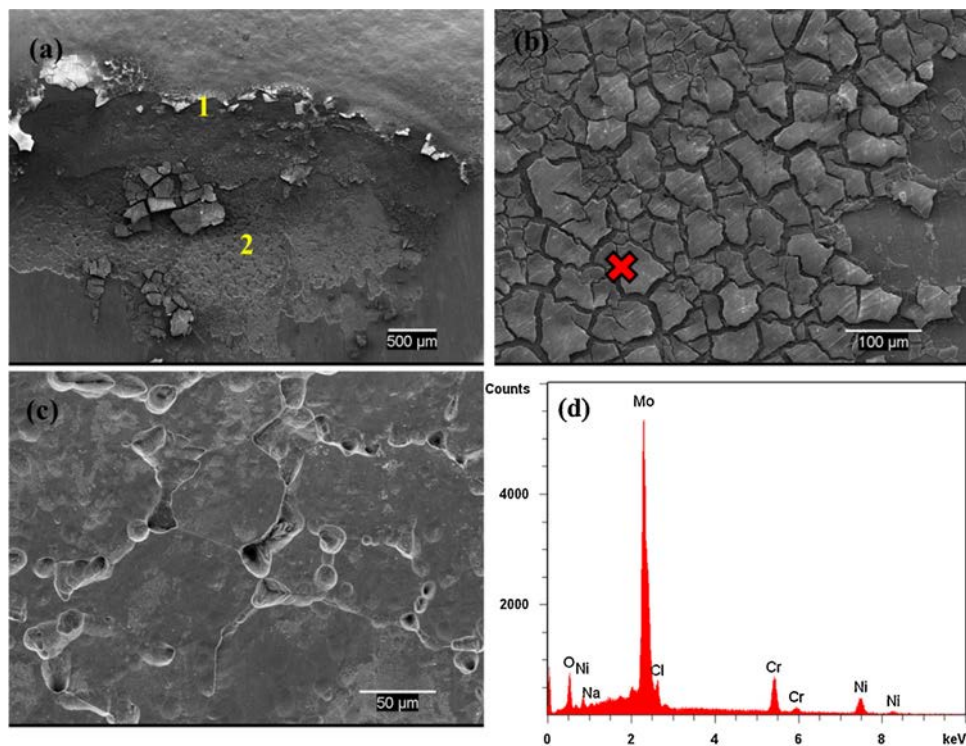

Fig. 8. SEM images recorded after corrosion at an applied current of 20 μA for 96 h in 5 M NaCl solution at 120 °C: (a) the crevice mouth and corroded regions within the crevice; (b) the corrosion product accumulated near the crevice mouth (area 1); (c) the intergranularly corroded alloy surface (area 2) and (d) EDS analysis of the corrosion products at the location marked with an X.
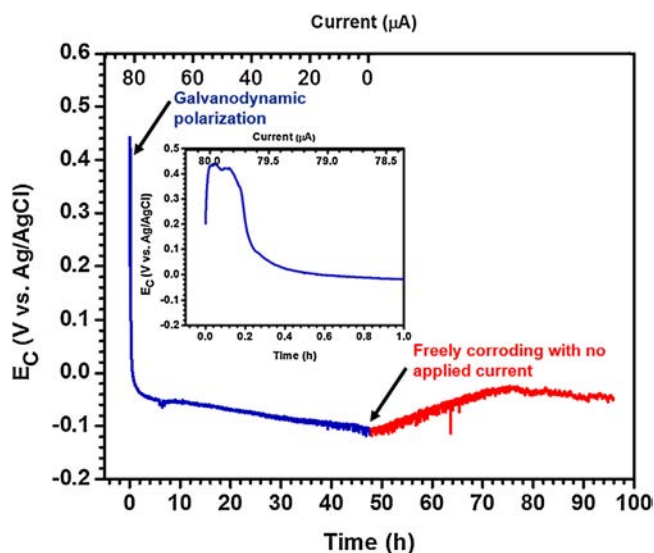
Fig. 10. E_C vs. time and current for galvanodynamic polarization of a BC1 creviced specimen in 5 M NaCl solution at 120 °C starting at $I = 80\,\mu$A with the current subsequently decreasing at a rate of $-1.667\,\mu$A/h. The experiment was followed by a measurement of E_C on open circuit after the applied current reached 0. The insert shows the details of the first hour of applied current.

Fig. 11. Potentiodynamic polarization curve obtained in deaerated 1 M HCl + 4 M NaCl solution at 120 °C.

expect the rate of propagation to slowly decrease to zero, at which point the crevice would be expected to repassivate.

Fig. 10 shows the response of E_C to the decreasing current. Once the current reached zero, E_C was measured for a further period of 50 h. The inset in the figure shows that the passive-to-active transition occurred in 10–12 min as observed for a constant applied current of 80 μA (Fig. 1). Fig. 11 shows a polarization curve recorded in a simulated crevice solution (deaerated 1 M HCl + 4 M NaCl) from E_{CORR} -50 mV to 1.1 $V_{Ag/AgCl}$. The active, passive and transpassive regions are clearly delineated. This curve shows that under the
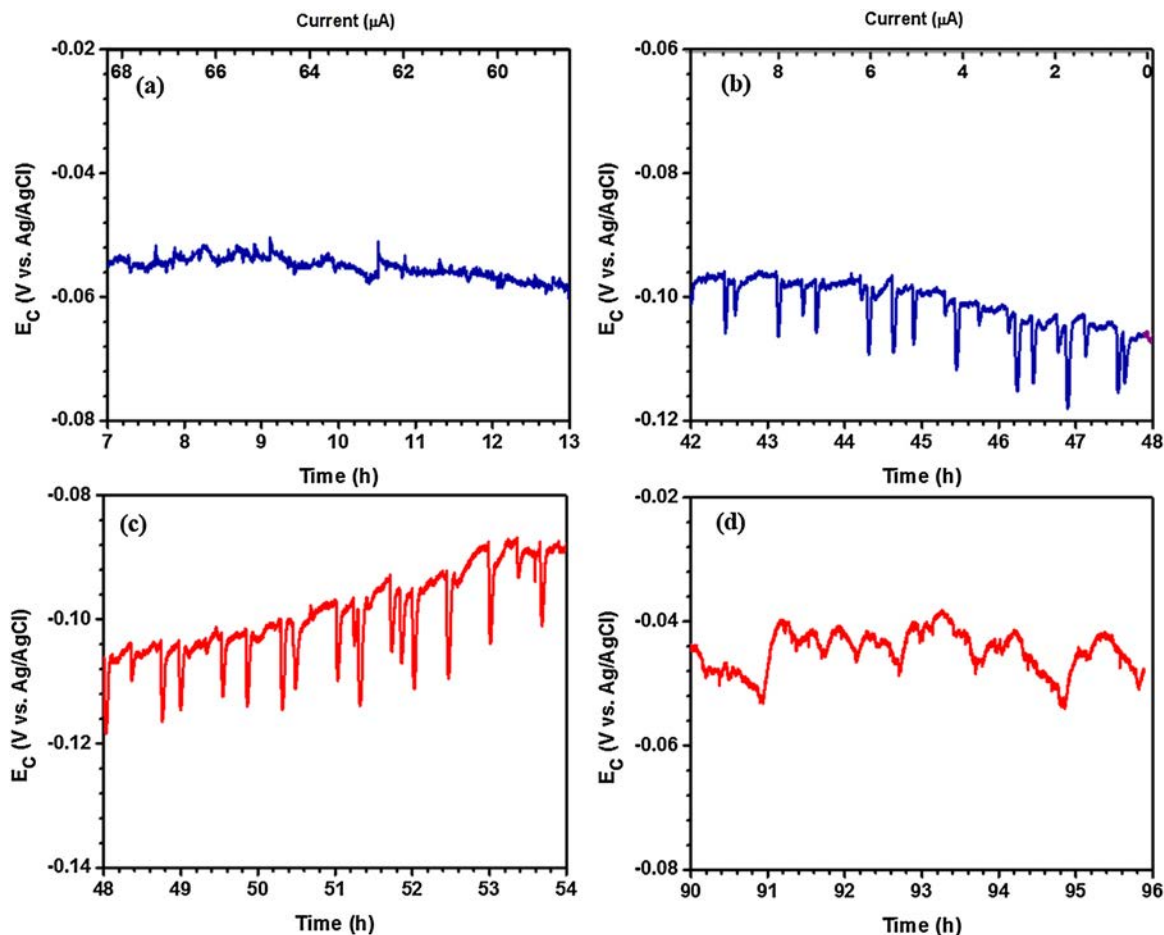

Fig. 12. (a) and (b), E_C –time plots recorded over various time periods of the galvanodynamic experiment in 5 M NaCl solution at 120 °C (Fig. 10); (c) and (d) E_C-time plots recorded over two time periods during the open circuit period of the experiment (Fig. 10).
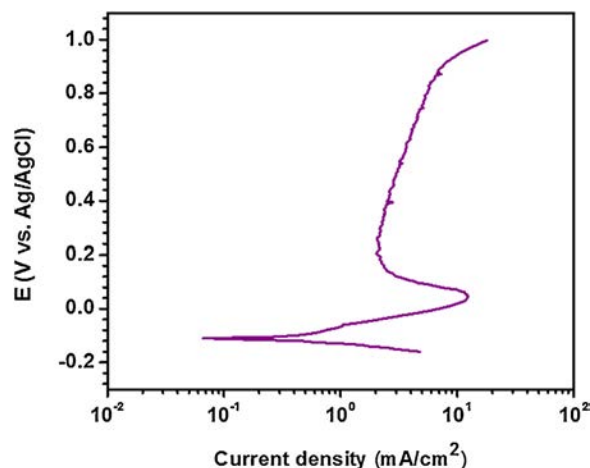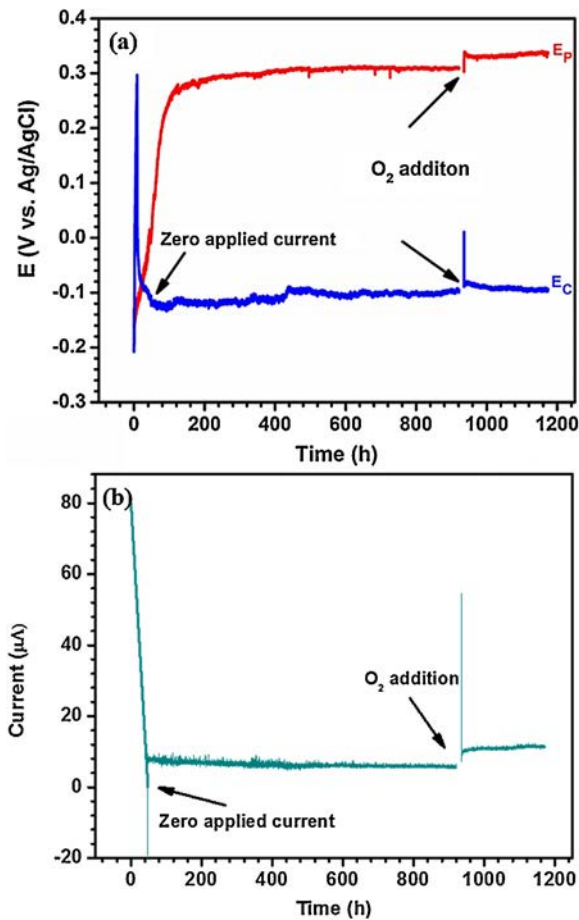
Fig. 13. (a) E_C, E_P, and (b) I_C as functions of time during a galvanodynamic crevice experiment (up to 48 h) followed by a subsequent period with the crevice galvanically-coupled to a large counter electrode (up to 1200 h). The experiment was performed in 5 M NaCl solution at 120 °C. The time at which the applied current reached zero and the time O$_2$ was added to the cell are indicated.

acidic conditions anticipated in the crevice the alloy can be considered to be in the active region for potentials ≤ 0.1 V and should have an $E_{CORR} \sim -0.1$ V. The corrosion current can be estimated with reference to the polarization curve by matching observed values of E_C to the polarization curve (Fig. 11) and estimating the associated current value. The current shows that crevice remains active showing no tendency to repassivate. However, the corrosion current values determined by this approach can only be considered estimates because the polarization curve represents the overall current only (i.e. sum of anodic and cathodic contributions at any potential) and it does not include the ohmic potential drop given by the tortuous path of the crevice.

As the current was decreased, E_C became significantly noisier, Fig. 10. This can be appreciated by comparing the minor fluctuations in the current range 68 µA to 58 µA, Fig. 12(a), with those in the current range 8–0 µA, Fig. 12(b). As the current approached zero, 10–12 mV excursions were observed. Expansion of the scale shows that these excursions lasted 3 to 5 minutes, suggesting that they involved small local chemical changes within the crevice. Once the current reached zero, E_C began to increase, achieving a steady-state value for the remaining 20 h of the experiment, Fig. 10. Additionally, the potential excursions that developed as the applied current approached zero persisted, Fig. 12(c), until the steady-state E_C was achieved, Fig. 12 (d). Even over this final steady-state period, E_C fluctuated over a 10–12 mV range but on a much longer time scale. This minimal increase in E_C over the 50 h open circuit
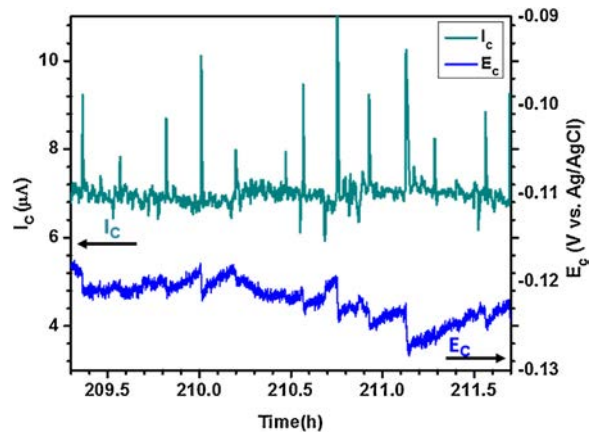

Fig. 14. An expanded view of transients on I_C and E_C during galvanic coupling experiment in 5 M NaCl solution at 120 °C between 210–212 h.

period ($t > 48$ h, Fig. 12(c) and (d)) suggests that some potential-determining locations within the crevice remained active despite the absence of an external current.

This is not surprising since it was previously shown [22] that >50% of crevice propagation is supported by the reduction of protons within active crevice locations. This was attributed to the extensive hydrolysis of the highly charged cations (Cr(VI), Mo(VI)) produced by anodic dissolution, yielding a critical crevice solution with an extremely low pH. Under these conditions even low concentrations of O$_2$ reduced on the external surface of the crevice could maintain the critical chemistry at a number of small locations within the crevice.

3.4. Galvanically coupled experiment

To determine whether the crevice remained active once the applied current was reduced to zero, a similar galvanodynamic experiment was conducted, starting at 80 µA with the current slowly decreased to zero (achieved after 48 h). Then, the creviced electrode was galvanically-coupled to a large counter electrode through a zero resistance ammeter, and the crevice current, I_C, and E_C recorded. Simultaneously, the potential, E_P, of a planar electrode was also monitored. E_P increased steadily to a value of ~ 0.26 V over the first 120 h, Fig. 13(a), before finally achieving a long term value (up to 920 h) of ~ 0.3 V confirming the establishment of passivity on this electrode.

The galvanodynamically activated crevice electrode had an E_C value of ~ -0.11 V on first coupling to the large counter electrode, which increased to ~ -0.095 V over the subsequent period of galvanic coupling (up to 920 h, Fig. 13(a)). That the crevice was active and still able to propagate is confirmed by the value of I_C which rapidly established a value of ~ 8 µA at the beginning of the galvanic coupling period and was sustained, decreasing only to 6 µA after 920 h, Fig. 13(b). The support of crevice propagation by O$_2$ reduction on the coupled electrode was demonstrated by the addition of O$_2$ to the cell after 920 h, which led to an increase of I_C to ~ 11 µA and of E_C by 10 mV to -0.105 V. The planar electrode also sensed the addition of O$_2$, E_P increasing to ~ 0.33 V, Fig. 13(a).

Closer inspection of the E_C and I_C –time plots during the galvanically-coupled period reveals the presence of coupled excursions, with rapid decreases in E_C being accompanied by sudden increases in I_C, Fig. 14. This behavior suggests the initiation of new active locations, expected to be located around the propagating perimeter of the damaged area. However, an initial surge in I_C lasted only ~ 1 min while E_C took ~ 6–10 min to return to the value prevailing prior to the excursion; i.e., the demand for current from the
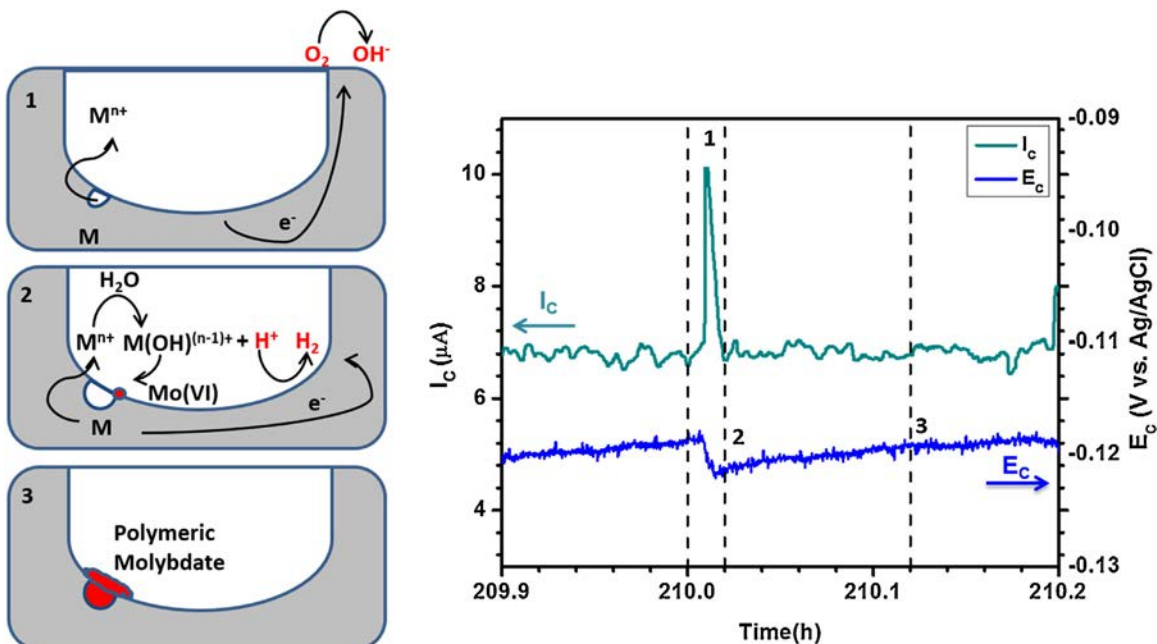
Fig. 15. Schematic showing the stages of (1) initiation of an active site at the periphery of the already crevice-corroded area; (2) propagation; and (3) stifling, and their corresponding I_C and E_C responses observed on a galvanically coupled crevice specimen corroding in 5 M NaCl solution at 120 °C.

external cathode is short but leads to a rapid local disturbance in electrochemical conditions.

Fig. 15 illustrates the probable mechanism behind the current-potential response observed in Fig. 14. Previously [22] it was shown that E_C is a function of the Mo content of a series of Ni–Cr–Mo alloys and almost independent of the external current supply. Thus, the most likely explanation for the coupled short I_C-long E_C excursions is that the initiation of a new active location leading to exposure of the substrate alloy initially demands external current for metal dissolution to occur. This external current is provided by the oxygen reduction reaction, as shown in stage 1 in Fig. 15. Subsequently, local acidity develops as the metal cations hydrolyze, allowing a switch from external current demand (causing the decrease in I_C) to internal cathodic support by H^+ reduction (stage 2). As metal dissolution continues soluble Ni and Cr diffuse out of the corroding site and molybdate accumulates, leading to the increase in E_C and the suppression of active dissolution (stage 3). Such small events would account for the observation that crevice corrosion damage on these alloys inevitably accumulates as small pits, often linked

along grain boundaries, Fig. 8, and containing molybdate deposits [42,46]. It should be noted that the internal H^+ reduction cannot diminish the critical chemistry solution inside the crevice due to the extent of hydrolysis of metal cations especially Cr(VI) and Mo(VI) as discussed elsewhere [22].

When the O_2 concentration is decreased, the occurrence of these individual coupled events continues, as illustrated in Fig. 16, which shows I_C and E_C recorded over the time interval 812–813 h. The constancy of the current (except for the excursions) confirms that these individual active locations are stifled by molybdate accumulation and do not lead to an expansion of the area within the crevice undergoing active propagation, which would be expected to lead to an increased demand for external current support.

4. Conclusions

The distribution of crevice corrosion damage incurred on the BC1 Ni–Cr–Mo alloy under galvanostatic conditions has been shown to redistribute within the creviced area depending on the value of the applied current. As previously observed for the high Cr-low Mo alloy, C22 (Ni-22Cr-13Mo(wt%)) damage on the low Cr-high Mo BC1 alloy (Ni-15Cr-22Mo(wt%)) spreads laterally across the creviced area rather than penetrating into it.

Increasing the rate of propagation galvanostatically led to a wider distribution but shallower penetration of corrosion damage. This wider distribution/decreased penetration was more marked on the BC1 alloy than previously observed on the C22 alloy. This confirms that the tendency to spread can be attributed to the higher Mo content of the former alloy which leads to the more rapid accumulation of molybdates at active locations. This deposition of molybdates stifles corrosion at these locations and leads to a redistribution of the current to the edges of the damaged area where propagation is maintained. This "self healing" quality makes it difficult to interpret the damage distribution in terms of the IR drop model for crevice corrosion.

When the current supporting crevice propagation is reduced galvanodynamically, the crevice remains in the active region even when the applied current has been reduced to zero. This indicates
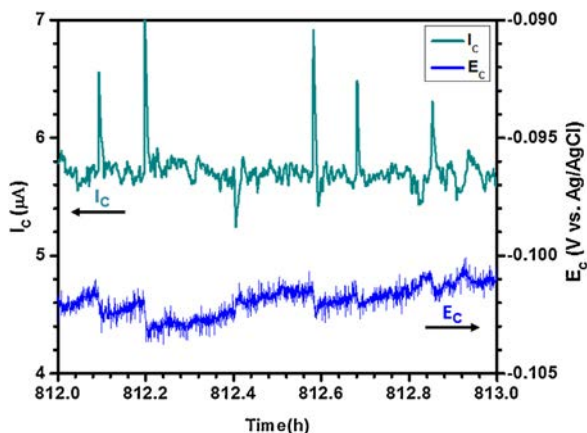

Fig. 16. An expanded view of transients in I_C and E_C during a galvanic coupling experiment in 5 M NaCl solution at 120 °C after 812 h.

that repassivation of the crevice does not occur readily, supporting our claim that propagation can be maintained by proton reduction inside the creviced region.

Switching to galvanic control (by coupling to a large counter electrode) confirmed that the crevice remained active, and propagation could be supported by oxygen reduction on the counter electrode, albeit at a slow rate. Provided that a supply of oxygen was maintained, no indication that the crevice would repassivate was observed, at least over a period of 1200 h.

Acknowledgements

References

[1] M.A. Rodríguez, R.M. Carranza, R.B. Rebak, Passivation and depassivation of alloy 22 in acidic chloride solutions, J. Electrochem. Soc. 157 (2010) C1–C8.

[2] D.C. Agarwal, N. Sridhar, Nickel Nickel Alloys, in: Uhlig's Corros Handb, Third, John Wiley and Sons, 2011, pp. 837–852.

[3] S.K. Ghosh, G.K. Dey, R.O. Dusane, A.K. Grover, Improved pitting corrosion behaviour of electrodeposited nanocrystalline Ni–Cu alloys in 3.0 wt.% NaCl solution, J.Alloys Compd. 426 (2006) 235–243.

[4] N.S. Zadorozne, C.M. Giordano, M.A. Rodríguez, R.M. Carranza, R.B. Rebak, Crevice corrosion kinetics of nickel alloys bearing chromium and molybdenum, Electrochim. Acta 76 (2012) 94–101.

[5] J.J. Gray, J.R. Hayes, G.E. Gdowski, B.E. Viani, C.A. Orme, Influence of solution pH, anion concentration, and temperature on the corrosion properties of alloy 22, J. Electrochem. Soc. 153 (2006) B61–B67.

[6] N.S. Meck, P. Crook, P.E. Manning, A new corrosion-resistant Ni–Mo–Cr alloy for the most versatile environments, Proc. Corrosion 2010, Paper No. 10336 NACE Int. (2010) 1–22.

[7] E.E.C. Hornus, C. Mabel Giordano, M.A. Rodríguez, R.M. Carranza, Effect of temperature on the crevice corrosion resistance of Ni–Cr–Mo alloys as engineered barriers in nuclear waste repositories, MRS Online Proc. Libr. 1475 (2012) 251–258.

[8] A.K. Mishra, S. Ramamurthy, M. Biesinger, D.W. Shoesmith, The activation/depassivation of nickel–chromium–molybdenum alloys in bicarbonate solution: Part I, Electrochim. Acta 100 (2013) 118–124.

[9] A.C. Lloyd, D.W. Shoesmith, N.S. McIntyre, J.J. Noël, Effects of temperature and potential on the passive corrosion properties of alloys C22 and C276, J. Electrochem. Soc. 150 (2003) B120–B130.

[10] M.A. Rodríguez, R.M. Carranza, Properties of the passive film on alloy 22 in chloride solutions obtained by electrochemical impedance, J. Electrochem. Soc. 158 (2011) C221–C230.

[11] X.H. Zhao, Y. Han, Z.Q. Bai, B. Wei, The experiment research of corrosion behaviour about Ni-based alloys in simulant solution containing H_2S/CO_2, Electrochim. Acta 56 (2011) 7725–7731.

[12] D.D. Macdonald, A. Sun, N. Priyantha, P. Jayaweera, An electrochemical impedance study of alloy-22 in NaCl brine at elevated temperature: II. Reaction mechanism analysis, J. Electroanal. Chem. 572 (2004) 421–431.

[13] F. Bocher, R. Huang, J.R. Scully, Prediction of critical crevice potentials for Ni–Cr–Mo alloys in simulated crevice solutions as a function of molybdenum content, Corrosion 66 (2010) 55002–55015.

[14] M. Rincón Ortíz, M.A. Rodríguez, R.M. Carranza, R.B. Rebak, Determination of the crevice corrosion stabilization and repassivation potentials of a corrosion-resistant alloy, Corrosion 66 (2010) 105002.

[15] A.K. Mishra, D.W. Shoesmith, Effect of alloying elements on crevice corrosion inhibition of nickel–Chromium–Molybdenum–Tungsten alloys under aggressive conditions: an electrochemical study, Corrosion 70 (2014) 721–730.

[16] P. Jakupi, J.J. Noël, D.W. Shoesmith, Crevice corrosion initiation and propagation on alloy-22 under galvanically-coupled and galvanostatic conditions, Corros. Sci. 53 (2011) 3122–3130.

[17] B.A. Kehler, G.O. Ilevbare, J.R. Scully, Crevice corrosion stabilization and repassivation behavior of alloy 625 and alloy 22, Corrosion 57 (2001) 1042–1065.

[18] E.C. Hornus, C.M. Giordano, M.A. Rodriguez, R.M. Carranza, R.B. Rebak, Effect of temperature on the crevice corrosion of nickel alloys containing chromium and molybdenum, J. Electrochem. Soc. 162 (2015) C105–C113.

[19] A. Tomio, M. Sagara, T. Doi, H. Amaya, N. Otsuka, T. Kudo, Role of alloyed molybdenum on corrosion resistance of austenitic Ni–Cr–Mo–Fe alloys in H_2S–Cl–environments, Corros. Sci. 98 (2015) 391–398.

[20] A.K. Mishra, G.S. Frankel, Crevice corrosion repassivation of alloy 22 in aggressive environments, Corrosion 64 (2008) 836–844.

[21] P. Jakupi, D. Zagidulin, J. Noël, D.W. Shoesmith, Crevice corrosion of Ni–Cr–Mo alloys, ECS Trans. 3 (2007) 259–271.

[22] N. Ebrahimi, P. Jakupi, J.J. Noël, D.W. Shoesmith, The role of alloying elements on the crevice corrosion behaviour of Ni–Cr–Mo alloys, Corrosion 71 (2015) 1441–1451.

[23] X. He, J.J. Noël, D.W. Shoesmith, Temperature dependence of crevice corrosion initiation on titanium Grade-2, J. Electrochem. Soc. 149 (2002) B440–B449.

[24] D. Shoesmith, J. Noël, D. Hardie, B. Ikeda, Hydrogen absorption and the lifetime performance of titanium nuclear waste containers, Corros. Rev. 18 (2000) 331–360.

[25] P. Jakupi, J.J. Noël, D.W. Shoesmith, The evolution of crevice corrosion damage on the Ni–Cr–Mo–W alloy-22 determined by confocal laser scanning microscopy, Corros. Sci. 54 (2012) 260–269.

[26] G.A. East, M.A. del Valle, Easy-to-make Ag/AgCl reference electrode, J. Chem. Educ. 77 (2000) 97.

[27] R.G. Kelly, J.R. Scully, D. Shoesmith, R.G. Buchheit, Electrochemical Techniques in Corrosion Science and Engineering, CRC Press, 2002.

[28] F. Bocher, J.R. Scully, Stifling of crevice corrosion and repassivation: cathode stifling of crevice corrosion and repassivation of stainless steel Fe-18Cr-8Ni-2Mo (wt%): cathode area versus controlled potential decreases assessed with a coupled multi-electrode array, Corrosion 71 (2015) 1049–1063.

[29] A.C. Lloyd, J.J. Noël, S. McIntyre, D.W. Shoesmith, Cr, Mo and W alloying additions in Ni and their effect on passivity, Electrochim. Acta 49 (2004) 3015–3027.

[30] D. Zagidulin, X. Zhang, J. Zhou, J.J. Noël, D.W. Shoesmith, Characterization of surface composition on Alloy 22 in neutral chloride solutions, Surf. Interface Anal 45 (2013) 1014–1019.

[31] D.D. Macdonald, Passivity–the key to our metals-based civilization, Pure Appl. Chem. 71 (1999) 951–978.

[32] R.S. Lillard, M.P. Jurinski, J.R. Scully, Crevice corrosion of alloy 625 in chlorinated astm artificial ocean water, Corrosion 50 (1994) 251–265.

[33] B.A. Kehler, J.R. Scully, Role of metastable pitting in crevices on crevice corrosion stabilization in alloys 625 and 22, Corrosion 61 (2005) 665–684.

[34] P. Jakupi, D. Zagidulin, J.J. Noël, D.W. Shoesmith, The impedance properties of the oxide film on the Ni–Cr–Mo alloy-22 in neutral concentrated sodium chloride solution, Electrochim. Acta 56 (2011) 6251–6259.

[35] J. Oldfield, W. Sutton, Crevice corrosion of stainless steels: II. Experimental studies, Br. Corros. J. 13 (1978) 104–111.

[36] J. Oldfield, W. Sutton, Crevice corrosion of stainless steels: I. A mathematical model, Br. Corros. J. 13 (1978) 13–22.

[37] H.W. Pickering, Whitney award lecture—1985: on the roles of corrosion products in local cell processes, Corrosion 42 (1986) 125–140.

[38] H.W. Pickering, Important early developments and current understanding of the IR mechanism of localized corrosion, J. Electrochem. Soc. 150 (2003) K1–13.

[39] M.I. Abdulsalam, H.W. Pickering, Effect of the applied potential on the potential and current distributions within crevices in pure nickel, Corros. Sci. 41 (1998) 351–372.

[40] M.I. Abdulsalam, H.W. Pickering, The effect of crevice-opening dimension on the stability of crevice corrosion for nickel in sulfuric acid, J. Electrochem. Soc. 145 (1998).

[41] X. Yuan, H.W. Pickering, The initial potential and current distributions of the crevice corrosion process, J. Electrochem. Soc. 140 (1993) 658–668.

[42] P. Jakupi, F. Wang, J.J. Noël, D.W. Shoesmith, Corrosion product analysis on crevice corroded alloy-22 specimens, Corros. Sci. 53 (2011) 1670–1679.

[43] P. Jakupi, J.J. Noël, D.W. Shoesmith, Intergranular corrosion resistance of (3 grain boundaries in alloy 22, Electrochem. Solid-State Lett. 13 (2010) C1–C3.

[44] C.A. Schuh, M. Kumar, W.E. King, Analysis of grain boundary networks and their evolution during grain boundary engineering, Acta Mater. 51 (2003) 687–700.

[45] S. Kobayashi, T. Maruyama, T. Tsurekawa, T. Watanabe, Grain boundary engineering based on fractal analysis for control of segregation-induced intergranular brittle fracture in polycrystalline nickel, Acta Mater. 60 (2012) 6200–6212.

[46] X. Shan, J.H. Payer, Characterization of the corrosion products of crevice corroded alloy 22, J. Electrochem. Soc. 156 (2009) C313–C321.